

Magnetic Weyl and Dirac Kondo semimetal phases in heterostructures

Seulgi Ok,¹ Markus Legner,² Titus Neupert,¹ and Ashley M. Cook¹

¹*Department of Physics, University of Zurich, Winterthurerstrasse 190, 8057 Zurich, Switzerland*
²*Institute for Theoretical Physics, ETH Zurich, 8093 Zurich, Switzerland*

We study a layered three-dimensional heterostructure in which two types of Kondo insulators are stacked alternately. One of them is the topological Kondo insulator SmB_6 , the other one an isostructural Kondo insulator AB_6 , where A is a rare-earth element, e.g., Eu, Yb, or Ce. We find that if the latter orders ferromagnetically, the heterostructure generically becomes a magnetic Weyl Kondo semimetal, while antiferromagnetic order can yield a magnetic Dirac Kondo semimetal. We detail both scenarios with general symmetry considerations as well as concrete tight-binding calculations and show that type-I as well as type-II magnetic Weyl/Dirac Kondo semimetal phases are possible in these heterostructures. Our results demonstrate that Kondo insulator heterostructures are a versatile platform for design of strongly correlated topological semimetals.

I. INTRODUCTION

Recent efforts to study phases defined by topologically-protected band structure degeneracies^{1–14} reflect their great potential for technological applications^{15,16} and for table-top experiments on quasiparticles both analogous to high-energy particles and beyond this framework^{17–25}. There is also a major undertaking to study these systems in the presence of correlations that suggests far richer physics beyond the weakly-correlated regime^{26–38}.

Heavy-fermion systems serve as an important guide in the study of correlations, and therefore of correlated topological phases: There is evidence these compounds host topological Kondo phases, which share the topological classification of weakly-correlated topological phases but with the essential difference that it is the strongly correlated Kondo effect that protects the topologically non-trivial state.³⁹ This area of research began with topological Kondo insulators^{40–56} but has more recently been extended to Chern Kondo insulators³⁹, topological crystalline Kondo insulators^{57,58}, Möbius Kondo insulators⁵⁹, Weyl Kondo semimetals due to inversion symmetry-breaking⁶⁰ and non-magnetic Dirac Kondo semimetals⁶¹.

The characterization of topological Kondo semimetals remains incomplete, however. The magnetic Weyl semimetal—a Weyl semimetal realized via time-reversal symmetry-breaking as opposed to inversion symmetry-breaking²—still lacks a counterpart phase, the magnetic Weyl Kondo semimetal, which is characterized by Weyl cones in the bulk electronic structure that are protected by the Kondo effect.

The magnetic Weyl semimetal—not the Weyl semimetal due to inversion symmetry-breaking—can be the elementary example of a Weyl semimetal in the sense that it may realize the minimum number of two Weyl cones². Experimental signatures of magnetic Weyl semimetals are simpler and may differ from those of Weyl semimetals due to inversion symmetry-breaking⁶². To date, there has only been one realization of the magnetic Weyl semimetal, and only in the presence of an applied magnetic field, while there have been

many experimental studies of Weyl semimetals due to inversion symmetry-breaking⁶³.

The magnetic Dirac Kondo semimetal is a state possessing Dirac cones, i.e., four-fold band degeneracies with linear dispersion in all directions in momentum space, in the bulk electronic structure when time-reversal symmetry is broken. These degeneracies emerge as a result of the Kondo effect and are protected by crystal symmetries of the magnetic space group. Magnetic Dirac semimetals have only been discussed very recently^{13,14,25,64}.

In this work, we show that both the magnetic Weyl Kondo semimetal and magnetic Dirac Kondo semimetal may, conveniently, be constructed from the topologically non-trivial surface states of the topological Kondo insulator samarium hexaboride (SmB_6), the most well-studied Kondo insulator and one of the best topological insulators when benchmarked by the minimal bulk conductivity⁶⁵. In this work, we explore the potential that SmB_6 and a family of isostructural materials AB_6 (where A is a rare-earth element or a combination of two dopants) hold for designing topological metals when stacked in a periodically repeating heterostructure [see Fig. 1 a)]. As these topological phases are constructed directly from the surface states of a topological Kondo insulator and these surface states are protected by the Kondo effect, these phases are topological Kondo metals.

We focus on symmetry-protected Weyl and Dirac cones brought about by ferromagnetic and antiferromagnetic order, respectively. While based on a proposal for weakly-correlated Weyl semimetals², our work goes beyond this proposal by (i) instead deriving topological semimetal phases from topologically non-trivial electronic structures resulting from intrinsically strongly-correlated Kondo physics³⁹, (ii) including the case of three dimensional magnetic Dirac Kondo semimetals, (iii) including realization of both type-I and type-II Weyl/Dirac Kondo semimetal phases, and (iv) utilizing the strong correlations of hexaborides as the sources of requisite magnetic orders as opposed to magnetic dopants^{66,67}. We note that SmB_6 furthermore exhibits evidence of exotic correlated topological surface states^{68–72}, which could enrich the physics of topological

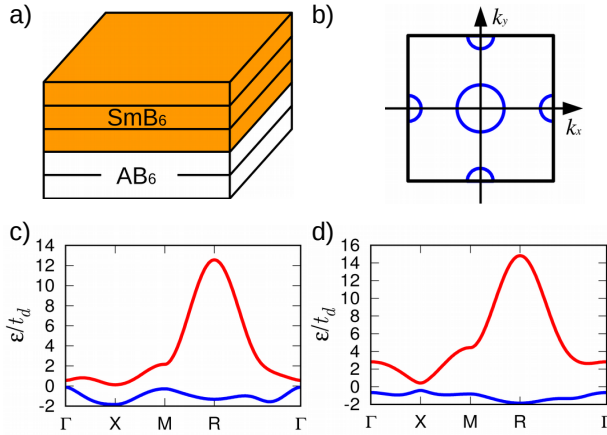


FIG. 1. a) Unit cell of the layered heterostructure consisting of a finite number of layers of each of two isostructural Kondo insulators, here the topological Kondo insulator SmB₆ and the trivial narrow-gap insulator AB₆. b) Schematic of the Fermi surface for some chemical potential μ intersecting the three Dirac cones on the (001) surface of SmB₆. Bulk electronic structures of the tight-binding models (6) for c) SmB₆ and d) an example AB₆ compound, respectively, arising from the hybridization between flat f bands and dispersive d bands, although the electronic structure of AB₆ could more generally also include p -bands near the Fermi level or just p - and d -bands near the Fermi level, or even be metallic⁷³, so long as the requisite symmetries and parent compound topologies are present, although this latter case is not ideal.

Kondo semimetals constructed from SmB₆ surface states.

II. MODEL FOR THE HETEROSTRUCTURE

A. Essential requirements of parent compounds

We consider a heterostructure made of periodic stackings of SmB₆ and another, possibly magnetic isostructural compound AB₆ [see Fig. 1 a)], candidates of which are discussed in Sec. IV. We will model parent compounds neglecting microscopic details as discussed in the next section. We consider one parent compound to be SmB₆, because it is the most established candidate for a topological Kondo insulator. While the topological nature of SmB₆ has been under debate⁷⁴, our work is based on the assumption that SmB₆ is a topological Kondo insulator. Our results also transfer to other topological Kondo insulators.

The realization of topological Kondo semimetals in such a heterostructure depends on the presence of the requisite symmetries and the topological insulator electronic structure of SmB₆, enabled by the Kondo effect. As we will show, appropriate magnetic order then induces magnetic Weyl or Dirac cones in the electronic structure. These Weyl or Dirac cones may appear even if AB₆ and (or) SmB₆—and with both (one) of them, the

heterostructure—is metallic.⁷³ Despite metallicity not being ideal, we stress that all experimentally-confirmed Weyl semimetals thus far have in fact been metallic rather than semimetallic⁷³.

B. Treatment of correlations

The topological properties of SmB₆ and AB₆ important for realization of topological Kondo semimetals can be realized without taking into account the full multiplet structure of the d - or f - orbitals. We thus consider a simplified model that ignores these details. As the essential difference between topological Kondo phases and weakly-correlated topological phases, however, is that the former are protected by bulk electronic structure resulting from the Kondo effect as opposed to weakly-correlated band structure³⁹, we must construct topological Kondo semimetal phases using a model for parent topological Kondo insulator compounds in which non-trivial topology emerges at *finite* correlation strength.

We therefore consider a lattice model for a topological Kondo insulator with cubic symmetry⁷⁵ for the description of the parent compounds SmB₆ and AB₆:

$$\begin{aligned} H = & \sum_{\gamma,s} \left[\sum_{\mathbf{r}} \tilde{\varepsilon}_{\gamma} c_{\gamma,\mathbf{r},s}^{\dagger} c_{\gamma,\mathbf{r},s} - \sum_{j=1}^3 \sum_{\langle \mathbf{r}, \mathbf{r}' \rangle_j} \tilde{t}_{\gamma}^{(j)} c_{\gamma,\mathbf{r},s}^{\dagger} c_{\gamma,\mathbf{r}',s} \right] \\ & + \sum_{\gamma,s,s',i} \sum_{\mathbf{r}} \left(i \tilde{V} c_{\gamma,\mathbf{r},s}^{\dagger} \sigma_{ss'}^i c_{\bar{\gamma},\mathbf{r}+\mathbf{e}_i,s'} + \text{H.c.} \right) \\ & + \sum_{\mathbf{r}} U c_{f,\mathbf{r},\uparrow}^{\dagger} c_{f,\mathbf{r},\uparrow} c_{f,\mathbf{r},\downarrow}^{\dagger} c_{f,\mathbf{r},\downarrow}. \end{aligned} \quad (1)$$

Here, $c_{\gamma,\mathbf{r},s}^{\dagger}$ ($c_{\gamma,\mathbf{r},s}$) denotes a creation (annihilation) operator for an electron in orbital $\gamma \in \{d, f\}$ with spin $s \in \{\uparrow, \downarrow\}$ on site \mathbf{r} of the cubic lattice, and $\langle \cdot \rangle_j$ for $j \in \{1, 2, 3\}$ denotes pairs of first (NN), second (NNN), and third neighbors (NNNN), respectively. The vectors \mathbf{e}_i connect nearest neighbors in the $i \in \{x, y, z\}$ directions. In the middle line of Eq. (1), $\bar{\gamma} = f$ ($\bar{\gamma} = d$) when $\gamma = d$ ($\gamma = f$). The parameters $\tilde{t}_{\gamma}^{(j)}$ stand for j -th nearest neighbor hopping integrals, $\tilde{\varepsilon}_{\gamma}$ the onsite-energy of γ band, and \tilde{V} the hybridization between f and d orbitals. The form of the hybridization as a parity-odd hopping term is a consequence of the opposite inversion eigenvalues of the d and f orbitals. Terms containing U govern interactions and reflect the assumption that f electrons locally interact via a Hubbard repulsion while the d electrons are non-interacting.

We consider the case where interactions strongly renormalize band parameters but low-energy excitations are described by well-defined Fermi-liquid quasiparticles. We can take advantage of previous work by Legner et al.⁷⁵ that used the Kotliar-Ruckenstein slave-boson scheme in the mean-field approximation⁷⁶ to treat interactions in the quasiparticle approximation to the periodic Anderson model^{76–79}, assuming a \mathbf{k} -independent self-energy

for the f -electrons of the Fermi liquid type $\Sigma_f(\omega) = a + b\omega + \mathcal{O}(\omega^2)$. The Fermi-liquid quasiparticles in such a state are then accurately described by a non-interacting Hamiltonian with renormalized parameters $\tilde{t}_f^{(j)} \rightarrow t_f^{(j)} = z^2 \tilde{t}_f^{(j)}$, $\tilde{V} \rightarrow V = z\tilde{V}$, $\tilde{\varepsilon}_f \rightarrow \varepsilon_f = \tilde{\varepsilon}_f + \lambda$, and $U \rightarrow 0$, while the others remain the same. The additional parameters z and λ are expressed by the self-energy expansion coefficients by $z = (1 - b)^{-1/2}$ and $\lambda = a/(1 - b)$, thus depend on the band parameters of the original Hamiltonian containing the quartic interaction terms between f -orbital electrons. The predominant effect of U is to move the f -electron band closer to the Fermi level, thereby enabling topological band inversion.

C. Low-energy effective theory for the heterostructure

Having discussed the effective non-interacting Hamiltonian that we use to describe bulk SmB_6 and AB_6 , we now study the mechanism by which three-dimensional (3D) bulk Weyl and Dirac cones arise in the heterostructure by weakly coupling the topological surface states of SmB_6 between consecutive interfaces within an effective theory for the surface states as expected in a heterostructure as shown in Fig. 1(a). Let us first consider both SmB_6 and the trivial insulator AB_6 to be nonmagnetic. In the surface Brillouin zone (BZ) of SmB_6 , there are three Dirac cones appearing at the two \bar{X} points $(\pi, 0), (0, \pi)$ and at the $\bar{\Gamma}$ point $(0, 0)$ [see Fig. 1(b)]. In the limit of decoupled interfaces, each interface between the two materials then hosts three Dirac cones, deriving from those appearing in the surface BZ of SmB_6 .

Weakly hybridizing these Dirac cones at $\Omega \in \{\bar{X}, \bar{\Gamma}\}$ with overlap integrals Δ_Ω and δ_Ω across the SmB_6 layer and the AB_6 layer, respectively, yields a low-energy effective theory for the heterostructure of the form

$$\begin{aligned} \mathcal{H}_\Omega(\mathbf{k}) = & v_F \tau^z (\hat{z} \times \boldsymbol{\sigma}) \cdot (\mathbf{k} - \mathbf{k}^\Omega) + \Delta_\Omega \tau^x \sigma^0 \\ & + \delta_\Omega (\tau^x \sigma^0 \cos k_z + \tau^y \sigma^0 \sin k_z) \end{aligned} \quad (2)$$

with $\mathbf{k}^{\bar{X}} = (\pi, \pi, 0)$ and $\mathbf{k}^{\bar{\Gamma}} = (0, 0, 0)$. Here, $\boldsymbol{\sigma}$ and $\boldsymbol{\tau}$ denote the vector of Pauli matrices in spin space and in the space of interfaces $\eta \in \{\text{upper, lower}\}$, respectively. Similarly, σ^0 and τ^0 are the 2×2 unit matrices in spin space and in the space of interfaces, respectively. For simplicity, we assume all three Dirac cones to be at the same energy and to be isotropic with the same Fermi velocity v_F ⁷¹.

We first discuss the low-energy theory without magnetic order. As translational symmetry is not broken in the xy plane, the findings of Ref.² apply separately for each of the Dirac cones at the surface of SmB_6 . Therefore, a band inversion occurs on the $\bar{\Gamma}$ -Z line when $|\Delta_{\bar{\Gamma}}| < |\delta_{\bar{\Gamma}}|$, and on the X-R line when $|\Delta_{\bar{X}}| < |\delta_{\bar{X}}|$. As we tune the number of SmB_6 layers (N_{TI}) and AB_6 layers (N_{BI}), the ratios $|\Delta_{\bar{\Gamma}}/\delta_{\bar{\Gamma}}|$ and $|\Delta_{\bar{X}}/\delta_{\bar{X}}|$ change, thus making it possible to observe multiple topologically distinct

phases. Depending on whether or not band inversions occur on the two different high-symmetry lines, we can distinguish four different phases [see Fig. 2 a): A weak topological insulator (WTI) if there is a band inversion along the X-R line, a strong topological insulator (STI₂) for a band inversion along the $\bar{\Gamma}$ -Z line, another strong topological insulator (STI₁) for band inversions on both lines, or a band insulator (BI) without any band inversions. Considering the extreme limits of either only SmB_6 or only AB_6 , we expect the system to be in the phases STI₁ and BI, respectively. Therefore, it is expected that the system will realize either of two phase transitions STI₁-WTI-BI or STI₁-STI₂-BI as we increase $N_{\text{BI}}/N_{\text{TI}}$ from 0 to ∞ [see Fig. 2 a)].

We now consider the heterostructure with magnetic order. In the case of ferromagnetic order in the \hat{z} direction, there is no coupling between Dirac cones centered around different points in the BZ, so we may consider each one individually with an additional term for the net magnetization in the \hat{z} direction:

$$\mathcal{H}_\Omega^{\text{FM}}(\mathbf{k}) = \mathcal{H}_\Omega(\mathbf{k}) + m \tau^0 \sigma^z. \quad (3)$$

The eigenvalues of this Hamiltonian are given by

$$E_{\alpha,\beta}^\Omega = \alpha \sqrt{v_F^2 (\tilde{k}_x^2 + \Delta \tilde{k}_y^2) + [m + \beta M_\Omega(k_z)]^2}, \quad (4a)$$

with

$$\tilde{k}_x = k_x - k_x^\Omega, \quad \tilde{k}_y = k_y - k_y^\Omega, \quad (4b)$$

$$M_\Omega(k_z) = \sqrt{\Delta_\Omega^2 + \delta_\Omega^2 + 2\delta_\Omega \Delta_\Omega \cos k_z}, \quad (4c)$$

where α and β can take the values ± 1 . Thus, at $k_x = k_x^\Omega$, $k_y = k_y^\Omega$, $m = \pm M_\Omega(k_z)$, we obtain Weyl cones.

As a second case, we discuss antiferromagnetic order with an ordering vector $\mathbf{Q} = (\pi, \pi, 0)$. (Note that Q_z is defined with respect to the unit cell of the heterostructure, not the lattice spacing of the comprising materials.) In that case, the surface Dirac cones at the two \bar{X} points are coupled, leading to the Hamiltonian

$$\mathcal{H}_{\bar{X}}^{\text{AFM}}(\mathbf{k}) = \rho^0 \mathcal{H}_{\bar{X}}(\mathbf{k}) + m \rho^x \tau^0 \sigma^z, \quad (5)$$

where $\boldsymbol{\rho}$ and ρ^0 are the vector of Pauli matrices and the 2×2 unit matrix in the space of the two Dirac cones at the different \bar{X} points, respectively. This Hamiltonian has the same eigenvalues as those given in Eq. (4) with $\Omega = \bar{X}$, but with an extra double degeneracy of each band.

The antiferromagnetic order breaks time-reversal symmetry T , but preserves the combination of T and a translation t_a by a displacement $a = (1, 0, 0)$ in units of the lattice constant. The symmetry (Tt_a) is represented by $-\mathcal{K} \rho^z \tau^0 \sigma^y$ (where \mathcal{K} represents complex conjugation) and in combination with inversion symmetry I leads to Kramer's degeneracy at each \mathbf{k} . In addition, the heterostructure has a C_4^z rotation symmetry that

protects Dirac cones on the C_4^z invariant lines, such as $k_x = k_y = 0$, as a crossing of two pairs of bands with different C_4^z eigenvalues. For finite $(\pi, \pi, 0)$ magnetic order and $\Delta/\delta \sim \pm 1$, bulk Dirac cones emerge in pairs near the A and M point in the folded BZ, respectively.

D. Lattice model

The effective model for the heterostructure showed that Weyl and Dirac cones can appear in the ferro- and antiferromagnetically ordered case, respectively, but it cannot be used to determine the strength of the hybridization terms Δ_Ω and δ_Ω . To determine which of the possible phases can be realized in the actual heterostructure, we now use the quasiparticle Hamiltonian for a topological Kondo insulator with cubic symmetry, which contains parameters renormalized by the Hubbard U^{75} :

$$H = \sum_{\gamma,s} \left[\sum_{\mathbf{r}} \varepsilon_{\gamma,\mathbf{r}} c_{\gamma,\mathbf{r},s}^\dagger c_{\gamma,\mathbf{r},s} - \sum_{j=1}^3 \sum_{\langle \mathbf{r}, \mathbf{r}' \rangle_j} t_\gamma^{(j)} c_{\gamma,\mathbf{r},s}^\dagger c_{\gamma,\mathbf{r}',s'} \right] + \sum_{\gamma,s,s',i} \sum_{\mathbf{r}} (iV c_{\gamma,\mathbf{r},s}^\dagger \sigma_{ss'}^i c_{\bar{\gamma},\mathbf{r}+e_i,s'} + \text{H.c.}) . \quad (6)$$

To model the heterostructure, we endow the onsite energies $\varepsilon_{\gamma,\mathbf{r}}$ with a spatial dependence to change their values between the two materials comprising the heterostructure. The parameter $\varepsilon_f - \varepsilon_d$ changes the bulk band topology of the translationally invariant model between normal insulator, weak topological insulator, and strong topological insulator^{75,80}. As discussed in Sec. II B, the effect of correlations is encoded in the renormalization of the model parameters: most notably, increasing the correlation strength induces a shift in ε_f and reduces V , $t_f^{(1)}$, and $t_f^{(2)}$ ⁷⁵.

The heterostructure is then modeled as N_{TI} layers of the topological Kondo insulator SmB₆, using the parameter set⁷⁵ $t_f^{(1)} = -0.1t_d^{(1)}$, $t_d^{(2)} = -0.4t_d^{(1)}$, $t_f^{(2)} = 0.04t_d^{(1)}$, $t_d^{(3)} = t_f^{(3)} = 0$, $V = 0.5t_d^{(1)}$, $\varepsilon_d = 1.76t_d^{(1)}$, $\varepsilon_f = -0.24t_d^{(1)}$, where we set $t_d^{(1)} = 100$ meV in order to produce the correct band gaps, and N_{BI} layers of a trivial Kondo insulator with the same parameters except for $\varepsilon_d = 4.02t_d^{(1)}$, $\varepsilon_f = -0.78t_d^{(1)}$, corresponding to our example AB₆. The bulk band structures of these two parameter sets are shown in Fig. 1 c) and d). The (topological) band gap of SmB₆ is then 24 meV, a value in good agreement with past work⁸¹. For AB₆, we choose a band gap of 84 meV.

III. RESULTS

A. Phase diagram at zero magnetization

We first explore the topology of the heterostructure in the absence of magnetic order. We fix the number of lay-

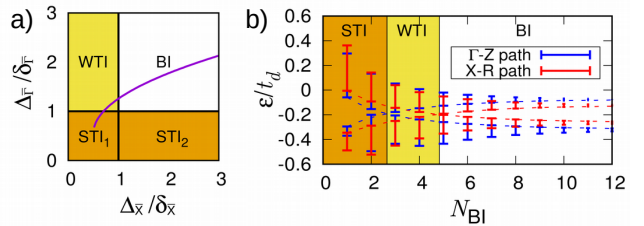


FIG. 2. Topological phases of the nonmagnetic heterostructure. a) Phase diagram of the effective model for the heterostructure based on the coupling of topological Dirac surface states. Depending on the strength of the couplings between the surface states, $\Delta_{\bar{\Gamma},\bar{X}}$ and $\delta_{\bar{\Gamma},\bar{X}}$, the heterostructure can realize a normal band insulator (BI), a weak topological insulator (WTI), or a strong topological insulator with (STI₁) or without (STI₂) nontrivial weak indices. b) Phase diagram of the tight-binding model for the heterostructure with a fixed number of 2 layers of SmB₆ and a variable number N_{BI} of layers of the trivial Kondo insulator AB₆. Vertical bars indicate the band widths of the highest valence and lowest conduction band along the high-symmetry lines Γ -Z and X-R. Topological transitions are accompanied by gap closings at the end of these lines, indicated by the dashed guides to the eye. The system follows a trajectory similar to the blue line in the phase diagram a) as N_{BI} is varied.

ers of SmB₆, N_{TI} ($N_{\text{TI}} = 2$ in our examples), and characterize the topology of the heterostructure as a function of the number of layers of AB₆, N_{BI} . We can therefore interpolate between the limits of the topological Kondo insulator SmB₆ for $N_{\text{BI}} = 0$ and YbB₆ for $N_{\text{BI}} \gg N_{\text{TI}}$. The chemical potential is fixed to lie between the two middle bands of the heterostructure dispersion, corresponding to half filling.

To show when band touchings occur, we compute where the minima and maxima of the middle two bands on high symmetry lines Γ -Z and X-R are located in energy as a function of the number of layers of AB₆. Furthermore, we compute the strong and weak \mathbb{Z}_2 topological indices to determine the topological phases between band touchings. A series of phase transitions STI₁-WTI-BI is detected between $N_{\text{BI}} = 2$ and 3, and between 4 and 5, respectively [see Fig. 2 b)]. We first focus on the former case and construct a phase diagram showing the number of Weyl cones formed between the two middle bands as a function of the number of AB₆ layers and the magnitude of the magnetization [see Fig. 3 a)].

B. Ferromagnetism and the magnetic Weyl Kondo semimetal

Ferromagnetic order could emerge via various mechanisms. In this work, we consider two cases: ferromagnetic order in SmB₆ or in the trivial Kondo insulator (corresponding to, e.g., ferromagnetic EuB₆).

We find four different phases depending on N_{BI} and m , corresponding to 0, 2, 4, and 6 Weyl cones present in the

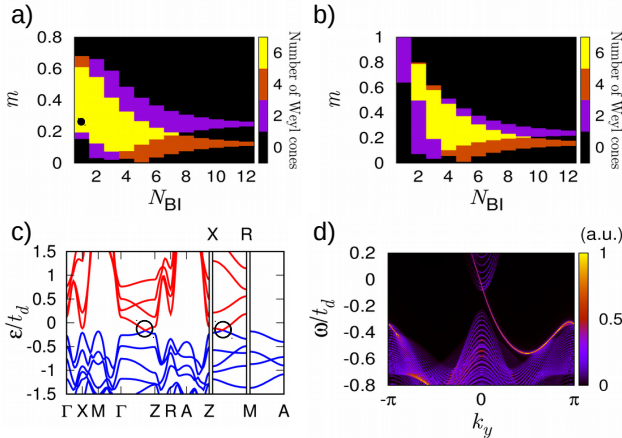


FIG. 3. Weyl semimetal phases of the ferromagnetic heterostructure. a), b) Phase diagrams indicating the number of Weyl cones between the highest valence and the lowest conduction band for ferromagnetic order a) in the SmB_6 and b) in the AB_6 layers. Here, m is the strength of the magnetization and the number of SmB_6 layers is fixed to 2. c) Band structure of the heterostructure for parameter values corresponding to the black circle in a). Weyl cones are indicated by black circles. d) Surface spectral function of the (100) surface for a slab geometry of the heterostructure in c) at $k_z = \pi$, showing a chiral mode belonging to a Fermi arc surface state.

system, which are located along the high-symmetry lines Γ -Z and X-R. Depending on the parameters, these Weyl cones can either be of type I or type II^{82,83}. A representative band structure for magnetization $m = 0.25t_d^{(1)}$ is shown in Fig. 3 c). We can understand the phase diagram structure as follows: The Dirac cones of the (001) surface of SmB_6 occur at the \bar{X} and $\bar{\Gamma}$ points in the surface BZ and each Dirac cone can yield a pair of Weyl cones for finite magnetization in the layering direction, as discussed in the section on the low-energy effective theory of the heterostructure. The offset in energy between the surface Dirac cones of SmB_6 means six Weyl cones emerge at intermediate magnetization from the $\bar{\Gamma}$ and also each \bar{X} surface Dirac cone. As N_{BI} increases, the band width of the middle bands decreases, finally eliminating this intermediate regime and generating two tails where Weyl cones appear either only around the X points (4 Weyl cones) or the Γ point (2 Weyl cones).

We also compute the spectral function of the heterostructure in a slab geometry, using again the magnetization $m = 0.25t_d^{(1)}$. With the heterostructure stacked in the \hat{z} direction, we open the system in the \hat{x} direction and compute the surface spectral function $A_{\text{surf}}(\omega, k_y, k_z) = \text{Im Tr} [\mathcal{G}(\omega, k_y, k_z) P_{\text{surf}}]$, where $\mathcal{G}(\omega, k_y, k_z)$ is the Green's function and P_{surf} the projector on one surface layer. This result is presented in Fig. 3 d), where a Fermi arc, a signature of a Weyl semimetal⁴, is clearly visible.

We can similarly compute the dispersion, phase diagram, and spectral function for the case of a net magnetization in the trivial Kondo insulator, $A = \text{Eu}$. The same

three topologically non-trivial phases—characterized by 2, 4, and 6 Weyl cones, respectively—that appear in Fig. 3 a) also occur in this second phase diagram, shown in Fig. 3 b).

C. Antiferromagnetism and the magnetic Dirac Kondo semimetal

Motivated by the low-energy model of the heterostructure for antiferromagnetic order, we now consider the full heterostructure Hamiltonian with finite magnetization in SmB_6 layers corresponding to antiferromagnetic order oriented in the stacking direction. We physically motivate this case as follows: There is evidence of antiferromagnetic order induced in bulk SmB_6 by compression^{66,67}. Also, $\text{Eu}_x\text{Ca}_{1-x}\text{B}_6$, where $x = 0.4$ and 0.6, was reported to show intrinsic antiferromagnetism below 3 K⁸⁴.

For the antiferromagnetic order, we add

$$\sum_{\gamma,s} \sum_{\mathbf{r} \in \text{TI/BI}} m_{\gamma,\mathbf{r},s}^{\text{AFM}} c_{\gamma,\mathbf{r},s}^\dagger c_{\gamma,\mathbf{r},s} \quad (7a)$$

to the Hamiltonian (6), where \mathbf{r} sums over either TI or BI layers depending on the case, and $m_{f,\mathbf{r},s}^{\text{AFM}} = s(-1)^{i+j+k} m'$ at $\mathbf{r} = i\mathbf{e}_x + j\mathbf{e}_y + k\mathbf{e}_z$. We take a particular form of $m_{d,\mathbf{r},s}^{\text{AFM}} = 0.2m_{f,\mathbf{r},s}^{\text{AFM}}$ if \mathbf{r} is in TI layers, and $m_{d,\mathbf{r},s}^{\text{AFM}} = m_{f,\mathbf{r},s}^{\text{AFM}}$ if \mathbf{r} is in BI layers, to express compression-based antiferromagnetism in topological Kondo insulator layers dominant in the f orbitals, as well as exciton-based antiferromagnetism that is neither predominantly of d or f orbital character^{85,86}, respectively. We also add an NNN hybridization

$$\sum_{\gamma,s,s',i} \sum_{\mathbf{r}} [iV' c_{\gamma,\mathbf{r},s}^\dagger (\boldsymbol{\sigma} \cdot \hat{\mathbf{d}}_i)_{ss'} c_{\gamma,\mathbf{r}+\hat{\mathbf{d}}_{i,s'}} + \text{H.c.}] \quad (7b)$$

in this section to isolate Dirac cones in the heterostructure bulk, where V' denotes the NNN hybridization coefficient, $\hat{\mathbf{d}}_i$, $i = 1, \dots, 6$, are taken from the set of six directed connections to the NNN sites, $\{\mathbf{e}_x \pm \mathbf{e}_y, \mathbf{e}_y \pm \mathbf{e}_z, \mathbf{e}_z \pm \mathbf{e}_x\}$, and $\hat{\mathbf{d}}_i$ denote the corresponding unit vectors. As representative values, we set $t_\gamma^{(3)} = 0.16t_\gamma^{(1)}$ and $V' = -0.2t_d^{(1)}$.

Two examples of Dirac semimetal dispersions of the heterostructure are shown in Fig. 4. Both type-I and type-II¹⁰ Dirac cones can occur in the full model, shown in Fig. 4 b) and d), respectively.

IV. AB_6 MATERIAL CANDIDATES

For the Weyl Kondo semimetal case, a promising candidate for AB_6 is EuB_6 as it displays the requisite ferromagnetic order^{87,88}. We note that there is evidence EuB_6 is metallic⁸⁹ as well as studies suggesting the compound

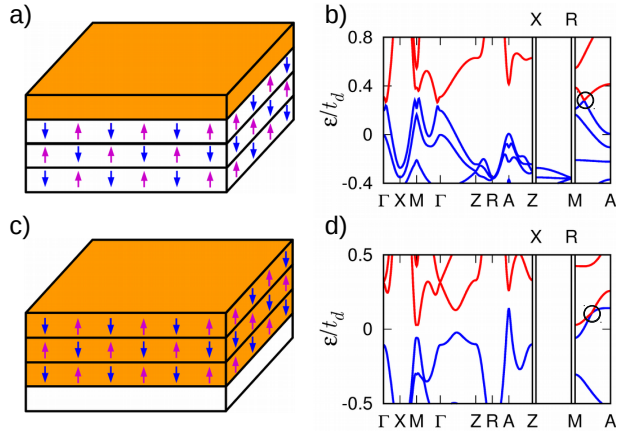


FIG. 4. Antiferromagnetic configurations for cases a) $N_{\text{TI}} = 1$, $N_{\text{BI}} = 3$, $m' = 1.0$ in BI layers, and c) $N_{\text{TI}} = 3$, $N_{\text{BI}} = 1$, $m' = 0.5$ in TI layers, and corresponding dispersions for the full heterostructure tight-binding Hamiltonian are shown in b) and d), respectively. A type-I (type-II) Dirac cone is visible on the M–A high-symmetry line in the BZ in subfigure b (d), highlighted with a black circle.

is a semimetal or a half-metallic semimetal⁹⁰, but emphasize again that this is not a problem for realization of the magnetic Weyl Kondo semimetal phase in practice: so long as the symmetries and parent compound topologies required for the magnetic Weyl Kondo semimetal phase are present, bulk Weyl cones will occur in the heterostructure near the Fermi level. We furthermore emphasize that Weyl cones in bulk dispersions have so far only been observed in what are actually metallic systems⁷³. We also note evidence that doping with Ca can push EuB₆ into an insulating state⁹¹.

For the magnetic Dirac Kondo semimetal case, we consider two promising candidates for AB₆. First, we discuss the potential of YbB₆ for this purpose. We note that the potential of YbB₆ as a topological Kondo insulator has been studied: the 4f and 5d bands of YbB₆ were proposed to be closest in energy to the Fermi level and the compound was proposed as a topological Kondo insulator candidate⁵⁸. Subsequently, it was suggested that the B 2p and Yb 5d bands of YbB₆ were actually closest in energy to the Fermi level and the material was proposed to be a topological insulator candidate due to inversion between predominantly p and d orbital character bands⁹². This agreed with other work^{93–95} showing that the binding energy of the Yb 4f 7/2 band is about 1 eV below the Fermi level. More recently, evidence was found, which suggests YbB₆ has bands with predominantly p- and d-orbital character near the Fermi level but that it is a *trivial insulator*⁹⁶, although the same study indicates the compound may become a p-d overlap semimetal under pressure. We therefore note that YbB₆ may satisfy the topology and symmetry requirements necessary to serve as AB₆ for construction of the

magnetic Dirac Kondo semimetal. Namely, it is topologically trivial⁹⁶, and we propose the magnetic structure of SmB₆ under pressure realizes the requisite symmetries for the magnetic Dirac Kondo semimetal phase.

CeB₆ is another promising candidate material: it exhibits a low-temperature magnetic phase^{97–105}, with anti-ferromagnetic order below 2.3 K¹⁰¹. Angle-resolved photoemission data¹⁰⁶ furthermore revealed the presence of 4f flat bands and dispersive 5d bands in the vicinity of the Fermi level. Transport studies indicate CeB₆ behaves as a Kondo metal¹⁰⁶, but we reiterate that the magnetic Dirac Kondo semimetal phase discussed here persists even if parent compounds become metallic, so long as the requisite symmetries and parent compound topologies hold, although this is not ideal⁷³.

V. DISCUSSION

We consider topological Kondo insulator heterostructures as platforms for the realization of magnetic Weyl and Dirac Kondo semimetal phases. We find ferromagnetism (antiferromagnetism) in the heterostructure generically realizes topologically-protected type-I and type-II Weyl (Dirac) cones sufficiently isolated from other states and proximate in energy to the Fermi level to realize type-I and type-II magnetic Weyl (Dirac) Kondo semimetal phases near half filling.

We note that thin films of SmB₆ have already been grown via molecular beam epitaxy (MBE)¹⁰⁷ and Kondo superlattices of other compounds have been grown via MBE for study of quantum criticality¹⁰⁸. Furthermore, evaporation of boron and most rare-earth lanthanides is possible at operating temperatures for effusion cells¹⁰⁹. Negative pressure on SmB₆ (lattice constant $a = 4.13 \text{ \AA}$ ^{110,111}) due to interfaces with EuB₆ ($a = 4.19 \text{ \AA}$ ¹¹²), YbB₆ ($a = 4.18 \text{ \AA}$ ⁹⁶), or CeB₆ ($a = 4.14 \text{ \AA}$ ¹¹³) may also permit the observation of the desired Kondo physics at much higher temperatures of up to 240 K as well as enhancement of one or both parent compound band gaps given observed effects of tensile strain in SmB₆⁷⁴.

ACKNOWLEDGMENTS

The authors gratefully acknowledge helpful discussions with Jason Hoffman, Manfred Sigrist, Ronny Thomale, Ian Affleck, Marcel Franz, Arun Paramekanti, Victor Galitski and Piers Coleman. This project was supported by the Swiss National Science Foundation (grant no. 200021_169061). AMC would also like to thank the Aspen Center for Physics, which is supported by National Science Foundation grant PHY-1066293, for hosting during some stages of this work.

- ¹ H. Weng, C. Fang, Z. Fang, B. A. Bernevig, and X. Dai, *Phys. Rev. X* **5**, 011029 (2015).
- ² A. A. Burkov and L. Balents, *Phys. Rev. Lett.* **107**, 127205 (2011).
- ³ S.-M. Huang, S.-Y. Xu, I. Belopolski, C.-C. Lee, G. Chang, B. Wang, N. Alidoust, G. Bian, M. Neupane, C. Zhang, *et al.*, *Nat. Commun.* **6** (2015).
- ⁴ S.-Y. Xu, I. Belopolski, N. Alidoust, M. Neupane, G. Bian, C. Zhang, R. Sankar, G. Chang, Z. Yuan, C.-C. Lee, S.-M. Huang, H. Zheng, J. Ma, D. S. Sanchez, B. Wang, A. Bansil, F. Chou, P. P. Shibayev, H. Lin, S. Jia, and M. Z. Hasan, *Science* **349**, 613 (2015).
- ⁵ B. Q. Lv, H. M. Weng, B. B. Fu, X. P. Wang, H. Miao, J. Ma, P. Richard, X. C. Huang, L. X. Zhao, G. F. Chen, Z. Fang, X. Dai, T. Qian, and H. Ding, *Phys. Rev. X* **5**, 031013 (2015).
- ⁶ Z. Wang, Y. Sun, X.-Q. Chen, C. Franchini, G. Xu, H. Weng, X. Dai, and Z. Fang, *Phys. Rev. B* **85**, 195320 (2012).
- ⁷ Z. K. Liu, B. Zhou, Y. Zhang, Z. J. Wang, H. M. Weng, D. Prabhakaran, S.-K. Mo, Z. X. Shen, Z. Fang, X. Dai, Z. Hussain, and Y. L. Chen, *Science* **343**, 864 (2014).
- ⁸ S. Borisenko, Q. Gibson, D. Evtushinsky, V. Zabolotnyy, B. Büchner, and R. J. Cava, *Phys. Rev. Lett.* **113**, 027603 (2014).
- ⁹ B.-J. Yang and N. Nagaosa, *Nat. Commun.* **5**, 4898 (2014).
- ¹⁰ T.-R. Chang, S.-Y. Xu, D. S. Sanchez, S.-M. Huang, G. Chang, C.-H. Hsu, G. Bian, I. Belopolski, Z.-M. Yu, X. Xu, C. Xiang, S. A. Yang, T. Neupert, H.-T. Jeng, H. Lin, and M. Zahid Hasan, ArXiv e-prints (2016), arXiv:1606.07555.
- ¹¹ S.-Y. Xu, C. Liu, S. K. Kushwaha, R. Sankar, J. W. Krizan, I. Belopolski, M. Neupane, G. Bian, N. Alidoust, T.-R. Chang, H.-T. Jeng, C.-Y. Huang, W.-F. Tsai, H. Lin, P. P. Shibayev, F.-C. Chou, R. J. Cava, and M. Z. Hasan, *Science* **347**, 294 (2015).
- ¹² S. M. Young and B. J. Wieder, ArXiv e-prints (2016), arXiv:1609.06738.
- ¹³ J. Wang, *Phys. Rev. B* **95**, 115138 (2017).
- ¹⁴ J. Wang, ArXiv e-prints (2017), arXiv:1701.00896.
- ¹⁵ D. I. Pikulin, A. Chen, and M. Franz, *Phys. Rev. X* **6**, 041021 (2016).
- ¹⁶ C. R. Rajamathi, U. Gupta, N. Kumar, H. Yang, Y. Sun, V. Süß, C. Shekhar, M. Schmidt, B. Yan, S. Parkin, *et al.*, ArXiv e-prints (2016), arXiv:1608.03783.
- ¹⁷ B. Bradlyn, J. Cano, Z. Wang, M. G. Vergniory, C. Felser, R. J. Cava, and B. A. Bernevig, *Science* **353** (2016).
- ¹⁸ B. J. Wieder, Y. Kim, A. M. Rappe, and C. L. Kane, *Phys. Rev. Lett.* **116**, 186402 (2016).
- ¹⁹ Z. Zhu, G. W. Winkler, Q. S. Wu, J. Li, and A. A. Soluyanov, *Phys. Rev. X* **6**, 031003 (2016).
- ²⁰ T. Bzdušek, Q. Wu, A. Rüegg, M. Sigrist, and A. A. Soluyanov, *Nature* **538**, 75 (2016).
- ²¹ C.-K. Chiu and A. P. Schnyder, *Phys. Rev. B* **90**, 205136 (2014).
- ²² L. S. Xie, L. M. Schoop, E. M. Seibel, Q. D. Gibson, W. Xie, and R. J. Cava, ArXiv e-prints (2015), arXiv:1504.01731.
- ²³ R. Yu, H. Weng, Z. Fang, X. Dai, and X. Hu, *Phys. Rev. Lett.* **115**, 036807 (2015).
- ²⁴ G. Bian, T.-R. Chang, R. Sankar, S.-Y. Xu, H. Zheng, T. Neupert, C.-K. Chiu, S.-M. Huang, G. Chang, I. Belopolski, *et al.*, *Nat. Commun.* **7** (2016).
- ²⁵ B. J. Wieder and C. L. Kane, *Phys. Rev. B* **94**, 155108 (2016).
- ²⁶ L. Lu, Z. Wang, D. Ye, L. Ran, L. Fu, J. D. Joannopoulos, and M. Soljačić, *Science* **349**, 622 (2015).
- ²⁷ R.-X. Zhang, J. A. Hutasoit, Y. Sun, B. Yan, C. Xu, and C.-X. Liu, *Phys. Rev. B* **93**, 041108 (2016).
- ²⁸ A. Sekine and K. Nomura, *Phys. Rev. B* **90**, 075137 (2014).
- ²⁹ R. Lundgren and G. A. Fiete, *Phys. Rev. B* **92**, 125139 (2015).
- ³⁰ J. González, *Phys. Rev. B* **92**, 125115 (2015).
- ³¹ V. V. Braguta, M. I. Katsnelson, A. Y. Kotov, and A. A. Nikolaev, *Phys. Rev. B* **94**, 205147 (2016).
- ³² L.-J. Zhai, P.-H. Chou, and C.-Y. Mou, *Phys. Rev. B* **94**, 125135 (2016).
- ³³ B. Roy and S. Das Sarma, *Phys. Rev. B* **94**, 115137 (2016).
- ³⁴ E. C. I. van der Wurff and H. T. C. Stoof, *Phys. Rev. B* **94**, 155118 (2016).
- ³⁵ B. Roy, P. Goswami, and V. Juricic, ArXiv e-prints (2016), arXiv:1610.05762.
- ³⁶ H. Wei, S.-P. Chao, and V. Aji, *Phys. Rev. Lett.* **109**, 196403 (2012).
- ³⁷ R. Schaffer, E. K.-H. Lee, Y.-M. Lu, and Y. B. Kim, *Phys. Rev. Lett.* **114**, 116803 (2015).
- ³⁸ M. Hermanns, K. O'Brien, and S. Trebst, *Phys. Rev. Lett.* **114**, 157202 (2015).
- ³⁹ H. Chen, X.-J. Liu, and X. C. Xie, *Phys. Rev. Lett.* **116**, 046401 (2016).
- ⁴⁰ M. Dzero, K. Sun, V. Galitski, and P. Coleman, *Phys. Rev. Lett.* **104**, 106408 (2010).
- ⁴¹ V. Alexandrov, M. Dzero, and P. Coleman, *Phys. Rev. Lett.* **111**, 226403 (2013).
- ⁴² J. Iaconis and L. Balents, *Phys. Rev. B* **91**, 245127 (2015).
- ⁴³ X.-Y. Feng, J. Dai, C.-H. Chung, and Q. Si, *Phys. Rev. Lett.* **111**, 016402 (2013).
- ⁴⁴ G. Li, Z. Xiang, F. Yu, T. Asaba, B. Lawson, P. Cai, C. Tinsman, A. Berkley, S. Wolgast, Y. S. Eo, D.-J. Kim, C. Kurdak, J. W. Allen, K. Sun, X. H. Chen, Y. Y. Wang, Z. Fisk, and L. Li, *Science* **346**, 1208 (2014).
- ⁴⁵ C.-H. Min, P. Lutz, S. Fiedler, B. Y. Kang, B. K. Cho, H.-D. Kim, H. Bentmann, and F. Reinert, *Phys. Rev. Lett.* **112**, 226402 (2014).
- ⁴⁶ H. Miyazaki, T. Hajiri, T. Ito, S. Kunii, and S.-i. Kimura, *Phys. Rev. B* **86**, 075105 (2012).
- ⁴⁷ S. Wolgast, C. Kurdak, K. Sun, J. W. Allen, D.-J. Kim, and Z. Fisk, *Phys. Rev. B* **88**, 180405 (2013).
- ⁴⁸ X. Zhang, N. P. Butch, P. Syers, S. Ziemak, R. L. Greene, and J. Paglione, *Phys. Rev. X* **3**, 011011 (2013).
- ⁴⁹ N. Xu, X. Shi, P. K. Biswas, C. E. Matt, R. S. Dhaka, Y. Huang, N. C. Plumb, M. Radović, J. H. Dil, E. Pomjakushina, K. Conder, A. Amato, Z. Salman, D. M. Paul, J. Mesot, H. Ding, and M. Shi, *Phys. Rev. B* **88**, 121102 (2013).
- ⁵⁰ M. Neupane, N. Alidoust, S.-Y. Xu, T. Kondo, Y. Ishida, D. J. Kim, C. Liu, I. Belopolski, Y. J. Jo, T.-R. Chang, H.-T. Jeng, T. Durakiewicz, L. Balicas, H. Lin, A. Bansil, S. Shin, Z. Fisk, and M. Z. Hasan, *Nat. Commun.* **4**, 2991 EP (2013).

- ⁵¹ E. Frantzeskakis, N. de Jong, B. Zwartsenberg, Y. K. Huang, Y. Pan, X. Zhang, J. X. Zhang, F. X. Zhang, L. H. Bao, O. Tegus, A. Varykhalov, A. de Visser, and M. S. Golden, *Phys. Rev. X* **3**, 041024 (2013).
- ⁵² T. Takimoto, *J. Phys. Soc. Jpn.* **80**, 123710 (2011).
- ⁵³ M.-T. Tran, T. Takimoto, and K.-S. Kim, *Phys. Rev. B* **85**, 125128 (2012).
- ⁵⁴ F. Lu, J. Z. Zhao, H. Weng, Z. Fang, and X. Dai, *Phys. Rev. Lett.* **110**, 096401 (2013).
- ⁵⁵ M. Dzero and V. Galitski, *J. Exp. Theor. Phys.* **117**, 499 (2013).
- ⁵⁶ X. Deng, K. Haule, and G. Kotliar, *Phys. Rev. Lett.* **111**, 176404 (2013).
- ⁵⁷ M. Y. Ye, J. W. Allen, and S. Kai, ArXiv e-prints (2013), arXiv:1307.7191.
- ⁵⁸ H. Weng, J. Zhao, Z. Wang, Z. Fang, and X. Dai, *Phys. Rev. Lett.* **112**, 016403 (2014).
- ⁵⁹ P.-Y. Chang, O. Erten, and P. Coleman, *Nat Phys advance online publication*, (2017).
- ⁶⁰ H.-H. Lai, S. E. Grefe, S. Paschen, and Q. Si, ArXiv e-prints (2016), arXiv:1612.03899.
- ⁶¹ X.-Y. Feng, H. Zhong, J. Dai, and Q. Si, ArXiv e-prints (2016), arXiv:1605.02380.
- ⁶² J. Cano, B. Bradlyn, Z. Wang, M. Hirschberger, N. P. Ong, and B. A. Bernevig, *Phys. Rev. B* **95**, 161306 (2017).
- ⁶³ M. Hirschberger, S. Kushwaha, Z. Wang, Q. Gibson, S. Liang, C. A. Belvin, B. A. Bernevig, R. J. Cava, and N. P. Ong, *Nat Mater* **15**, 1161 (2016).
- ⁶⁴ P. Tang, Q. Zhou, G. Xu, and S.-C. Zhang, *Nat. Phys.* **12**, 1100 (2016).
- ⁶⁵ A. Rakoski, Y. S. Eo, K. Sun, and C. Kurdkar, ArXiv e-prints (2017), arXiv:1702.02619.
- ⁶⁶ A. Barla, J. Derr, J. P. Sanchez, B. Salce, G. Lapertot, B. P. Doyle, R. Rüffer, R. Lengsdorf, M. M. Abd-Elmeguid, and J. Flouquet, *Phys. Rev. Lett.* **94**, 166401 (2005).
- ⁶⁷ J. Derr, G. Knebel, D. Braithwaite, B. Salce, J. Flouquet, K. Flachbart, S. Gabáni, and N. Shitsevalova, *Phys. Rev. B* **77**, 193107 (2008).
- ⁶⁸ Y. Nakajima, P. Syers, X. Wang, R. Wang, and J. Paglione, *Nat. Phys.* **12**, 213 (2016).
- ⁶⁹ A. Thomson and S. Sachdev, *Phys. Rev. B* **93**, 125103 (2016).
- ⁷⁰ V. Alexandrov, P. Coleman, and O. Erten, *Phys. Rev. Lett.* **114**, 177202 (2015).
- ⁷¹ B. Roy, J. Hofmann, V. Stanev, J. D. Sau, and V. Galitski, *Phys. Rev. B* **92**, 245431 (2015).
- ⁷² P. Nikolić, *Phys. Rev. B* **90**, 235107 (2014).
- ⁷³ B. Yan and C. Felser, *Annual Review of Condensed Matter Physics* **8**, 337 (2017), <https://doi.org/10.1146/annurev-conmatphys-031016-025458>.
- ⁷⁴ A. Stern, M. Dzero, V. M. Galitski, Z. Fisk, and J. Xia, ArXiv e-prints (2016), arXiv:1607.07454.
- ⁷⁵ M. Legner, A. Rüegg, and M. Sigrist, *Phys. Rev. B* **89**, 085110 (2014).
- ⁷⁶ G. Kotliar and A. E. Ruckenstein, *Phys. Rev. Lett.* **57**, 1362 (1986).
- ⁷⁷ N. Read and D. M. Newns, *Journal of Physics C: Solid State Physics* **16**, L1055 (1983).
- ⁷⁸ P. Coleman, *Phys. Rev. B* **29**, 3035 (1984).
- ⁷⁹ T. M. Rice and K. Ueda, *Phys. Rev. Lett.* **55**, 995 (1985).
- ⁸⁰ M. Dzero, J. Xia, V. Galitski, and P. Coleman, *Annu. Rev. Condens. Matter Phys.* **7**, 249 (2016).
- ⁸¹ T.-R. Chang, T. Das, P.-J. Chen, M. Neupane, S.-Y. Xu, M. Z. Hasan, H. Lin, H.-T. Jeng, and A. Bansil, *Phys. Rev. B* **91**, 155151 (2015).
- ⁸² A. A. Soluyanov, D. Gresch, Z. Wang, Q. Wu, M. Troyer, X. Dai, and B. A. Bernevig, *Nature* **527**, 495 (2015).
- ⁸³ Y. Xu, F. Zhang, and C. Zhang, *Phys. Rev. Lett.* **115**, 265304 (2015).
- ⁸⁴ J.-S. Rhyee, B. Oh, and B. Cho, *J. Korean Phys. Soc.* **44**, 1509 (2004).
- ⁸⁵ S. Murakami, R. Shindou, N. Nagaosa, and A. S. Mishchenko, *Phys. Rev. B* **66**, 184405 (2002).
- ⁸⁶ M. Zhitomirsky, T. Rice, and V. Anisimov, *Nature* **402**, 251 (1999).
- ⁸⁷ L. Degiorgi, E. Felder, H. R. Ott, J. L. Sarrao, and Z. Fisk, *Phys. Rev. Lett.* **79**, 5134 (1997).
- ⁸⁸ S. Süllow, I. Prasad, M. C. Aronson, J. L. Sarrao, Z. Fisk, D. Hristova, A. H. Lacerda, M. F. Hundley, A. Vigliante, and D. Gibbs, *Phys. Rev. B* **57**, 5860 (1998).
- ⁸⁹ J. E. Hirsch, *Phys. Rev. B* **59**, 436 (1999).
- ⁹⁰ J. Kuneš and W. E. Pickett, *Phys. Rev. B* **69**, 165111 (2004).
- ⁹¹ R. R. Urbano, P. G. Pagliuso, C. Rettori, P. Schlottmann, J. L. Sarrao, A. Bianchi, S. Nakatsuji, Z. Fisk, E. Velazquez, and S. B. Oseroff, *Phys. Rev. B* **71**, 184422 (2005).
- ⁹² M. Neupane, S.-Y. Xu, N. Alidoust, G. Bian, D. J. Kim, C. Liu, I. Belopolski, T.-R. Chang, H.-T. Jeng, T. Durakiewicz, H. Lin, A. Bansil, Z. Fisk, and M. Z. Hasan, *Phys. Rev. Lett.* **114**, 016403 (2015).
- ⁹³ A. Kakizaki, A. Harasawa, T. Kinoshita, T. Ishii, T. Nanba, and S. Kunii, *Physica B: Condensed Matter* **186**, 80 (1993).
- ⁹⁴ M. Xia, J. Jiang, Z. R. Ye, Y. H. Wang, Y. Zhang, S. D. Chen, X. H. Niu, D. F. Xu, F. Chen, X. H. Chen, B. P. Xie, T. Zhang, and D. L. Feng, *EP* **4**, 5999 EP (2014).
- ⁹⁵ E. Frantzeskakis, N. de Jong, J. X. Zhang, X. Zhang, Z. Li, C. L. Liang, Y. Wang, A. Varykhalov, Y. K. Huang, and M. S. Golden, *Phys. Rev. B* **90**, 235116 (2014).
- ⁹⁶ C.-J. Kang, J. D. Denlinger, J. W. Allen, C.-H. Min, F. Reinert, B. Y. Kang, B. K. Cho, J.-S. Kang, J. H. Shim, and B. I. Min, *Phys. Rev. Lett.* **116**, 116401 (2016).
- ⁹⁷ A. van Deursen, Z. Fisk, and A. de Vroomen, *Solid State Communications* **44**, 609 (1982).
- ⁹⁸ N. Harrison, D. W. Hall, R. G. Goodrich, J. J. Vuillemin, and Z. Fisk, *Phys. Rev. Lett.* **81**, 870 (1998).
- ⁹⁹ A. A. Teklu, R. G. Goodrich, N. Harrison, D. Hall, Z. Fisk, and D. Young, *Phys. Rev. B* **62**, 12875 (2000).
- ¹⁰⁰ D. Hall, Z. Fisk, and R. G. Goodrich, *Phys. Rev. B* **62**, 84 (2000).
- ¹⁰¹ O. Zaharko, P. Fischer, A. Schenck, S. Kunii, P.-J. Brown, F. Tasset, and T. Hansen, *Phys. Rev. B* **68**, 214401 (2003).
- ¹⁰² R. G. Goodrich, D. P. Young, D. Hall, L. Balicas, Z. Fisk, N. Harrison, J. Betts, A. Migliori, F. M. Woodward, and J. W. Lynn, *Phys. Rev. B* **69**, 054415 (2004).
- ¹⁰³ V. P. Plakhty, L. P. Regnault, A. V. Goltsev, S. V. Gavrilov, F. Yakhou, J. Flouquet, C. Vettier, and S. Kunii, *Phys. Rev. B* **71**, 100407 (2005).
- ¹⁰⁴ G. Friemel, Y. Li, A. V. Dukhnenko, N. Y. Shitsevalova, N. E. Sluchanko, A. Ivanov, V. B. Filipov, B. Keimer, and D. S. Inosov, *EP* **3**, 830 EP (2012).
- ¹⁰⁵ H. Jang, G. Friemel, J. Ollivier, A. V. Dukhnenko, N. Y. Shitsevalova, V. B. Filipov, B. Keimer, and D. S. Inosov, *Nat Mater* **13**, 682 (2014).

- ¹⁰⁶ M. Neupane, N. Alidoust, I. Belopolski, G. Bian, S.-Y. Xu, D.-J. Kim, P. P. Shibayev, D. S. Sanchez, H. Zheng, T.-R. Chang, H.-T. Jeng, P. S. Riseborough, H. Lin, A. Bansil, T. Durakiewicz, Z. Fisk, and M. Z. Hasan, *Phys. Rev. B* **92**, 104420 (2015).
- ¹⁰⁷ H. Shishido, Y. Yoneda, T. Yoshida, S. Noguchi, and T. Ishida, *Physics Procedia* **75**, 405 (2015).
- ¹⁰⁸ T. Ishii, R. Toda, Y. Hanaoka, Y. Tokiwa, M. Shimozawa, Y. Kasahara, R. Endo, T. Terashima, A. H. Nevidomskyy, T. Shibauchi, and Y. Matsuda, *Phys. Rev. Lett.* **116**, 206401 (2016).
- ¹⁰⁹ J. Hoffman, private communication.
- ¹¹⁰ J. Jiang, S. Li, T. Zhang, Z. Sun, F. Chen, Z. R. Ye, M. Xu, Q. Q. Ge, S. Y. Tan, X. H. Niu, M. Xia, B. P. Xie, Y. F. Li, X. H. Chen, H. H. Wen, and D. L. Feng, *Nat. Commun.* **4**, 3010 (2013).
- ¹¹¹ S. Rößler, T.-H. Jang, D.-J. Kim, L. H. Tjeng, Z. Fisk, F. Steglich, and S. Wirth, *Proc. Natl. Acad. Sci. USA* **111**, 4798 (2014).
- ¹¹² M. Kreissl and W. Nolting, *Phys. Rev. B* **72**, 245117 (2005).
- ¹¹³ M. I. A. J., and T. P, *Modeling and Numerical Simulation of Material Science* **3**, 158 (2013).